ACS APPLIED MATERIALS & INTERFACES

Letter

www.acsami.org

One-Step Surface Doping of Organic Nanofibers to Achieve High Dark Conductivity and Chemiresistor Sensing of Amines

Helin Huang,[†] Dustin E. Gross,[‡,§] Xiaomei Yang,[†] Jeffrey S. Moore,*[,‡] and Ling Zang*[,†]

[†]Department of Materials Science and Engineering, University of Utah, Salt Lake City, Utah 84108, United States

[‡]Departments of Chemistry and Materials Science and Engineering, University of Illinois at Urbana−Champaign, Urbana, Illinois 61801, United States

Supporting Information

ABSTRACT: High dark electrical conductivity was obtained for a p-type organic nanofibril material simply through a one-step surface doping. The nanofibril composite thus fabricated has been proven robust under ambient conditions. The high conductivity, combined with the intrinsic large surface area of the nanofibers, enables development of chemiresistor sensors for trace vapor detection of amines, with detection limit down to sub-parts per billion range.

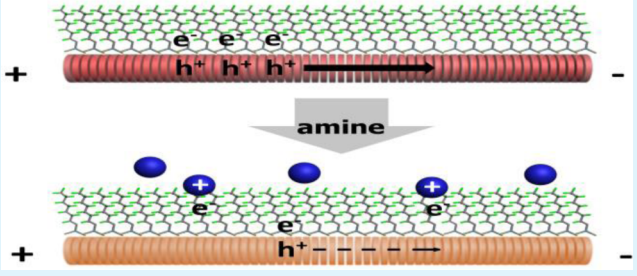

KEYWORDS: *organic nanofiber, p-type materials, surface doping, high conductivity, sensors, vapor detection*

INTRODUCTION

Organic semiconductor nanomaterials have gained increasing research interest due to their broad applications in photodetectors,[1−5] sensors,[6−8] and photovoltaics.[9−11] These materials are superior to their inorganic counterparts regarding synthetic variability, low temperature, and solution processing ability, and the feasibility of fabrication into lightweight, flexible, and low-cost devices.[12−14] However, most organic materials suffer from their intrinsically low charge carrier density and mobility. Current work to improve conductivity has involved blending electron donor (D) and acceptor (A) molecules into bulk phase heterojunctions, as evidenced in organic photovoltaics. In general, these D−A systems provide efficient photoinduced charge separation, although further charge transport is often limited by the intermolecular arrangement disordering and/or mesoscopic grain boundaries.[4,15]

Recently, we have developed a simple approach to fabricate nanofibril D−A heterojunctions, wherein the A molecules were assembled through $\pi-\pi$ stacking interaction into nanofibers, and the D component was coated on the nanofiber surface via drop-casting.[16] The strong hydrophobic interdigitation between the side chains of D and A produces an interface that is optimal for photoinduced charge separation. Moreover, the intermolecular $\pi-\pi$ stacking along the long axis of nanofiber facilitates the long-range charge transport through π-delocalization.[17−22] This continuous charge transport pathway, in combination with the wide D−A interfacial contact intrinsic to the nanofibril structure, makes nanofibril heterojunctions an ideal approach to highly photoconductive organic materials. However, it still remains challenging to achieve high dark conductivity for organic nanomaterials using this simple coating methodology.

In this work, we report on a new nanofibril heterojunction structure that composes of nanofibers (assembled from a D molecule) coated with a monolayer of A molecule. As shown in Scheme 1, D is a decyl substituted carbazole-cornered, arylene-ethynylene tetracyclic π-conjugated molecule (DTC), and A is (tridecafluoro-1,1,2,2-tetrahydrooctyl)trichlorosilane (FTS), which has proven to be effective to form a well-defined

Scheme 1. Molecular Structures of DTC, TDTC, FTS, and OTS

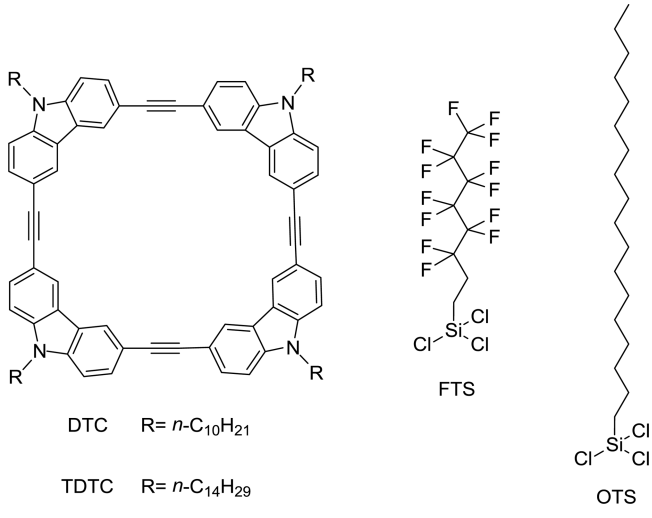

Received: June 21, 2013
Accepted: August 8, 2013
Published: August 8, 2013

dx.doi.org/10.1021/am402420g | ACS Appl. Mater. Interfaces 2013, 5, 7704−7708

monolayer on an organic material substrate under ambient conditions.[23,24] Remarkably, due to the strong redox (charge transfer) interaction between DTC and FTS, the nanofibril junction thus fabricated demonstrated high conductivity even without light illumination. The high dark conductivity makes this material suitable for applications in chemiresistor sensors for detection of volatile organic compounds (VOCs), particularly amines.

EXPERIMENTAL SECTION

Materials. All solvents and reagents were purchased from Sigma-Aldrich and used without purification. Synthesis and purification of DTC and TDTC macrocyclic molecules followed previously published methods and procedures.[25,26]

Fabrication of Nanofibers and Devices. Fabrication of nanofibers: 0.5 mL of 15 μM chloroform solution of DTC was injected rapidly into 5 mL of ethanol in a test tube. Nanofibers were produced immediately through precipitation driven self-assembly. The suspension was then aged in the refrigerator for 24 h to achieve more uniform nanofibers. The nanofibers thus generated can be transferred onto the surface by drop-casting method. Typically, after removing the excess solvent in the nanofiber suspension, 0.2 mL of such suspension was drop-casted onto a 5 mm × 5 mm glass substrate, followed by fast solvent evaporation in fume hood under ambient condition. The glass slide was first cleaned in acetone and isopropanol for 3 min each in an ultrasonic bath, and then cleaned with a piranha solution (70 vol % H_2SO_4:30 vol % 30% H_2O_2) for 20 min, followed by rinsing with deionized water and drying in air flow. The glass supported nanofibers thus made are suited for microscopy, optical and contact angle measurements.

Preparation of thin-film of TDTC: 0.5 mL of 15 μM chloroform solution of TDTC was drop-cast onto a 5 mm × 5 mm silicon wafer covered with 300 nm thick SiO_2, followed by fast solvent evaporation in fume hood.

Surface coating of FTS was performed using a vapor deposition procedure (see Figure S1 in the Supporting Information) that was previously developed by others.[23] Briefly, the nanofibers predeposited on a substrate was placed in a vacuum chamber (volume ~25 cm^3); a small container (volume ~5 cm^3) with a few drops of FTS placed in a different chamber separate from the vacuum chamber by a three-way valve that was connected with a membrane pump (BUCHI V500P). The vacuum chamber was evacuated first to reach the maximal vacuum level. Then, the FTS chamber was connected to the vacuum chamber through the three-way valve, to start the vapor diffusion of FTS. The vapor deposition process was completed in about 5 h.

Single pair electrodes were fabricated on a highly doped p-type silicon wafer covered with 300-nm-thick thermal oxide film. Using the traditional photolithography and lift-off approach, 30 nm thick Au/Cr electrode pairs were patterned on the wafer with a gap of 5 μm in width and 10 μm in length. Onto the electrode-pair thus fabricated the nanofibers can be deposited by drop-casting, the same procedure as described above for the deposition on glass substrate. This small volume drop-casting method produced devices that demonstrated quite good reproducibility, i.e., only slight variation in electrical current was observed between the different batches of devices (see Figure S9 in the Supporting Information).

Materials Characterization. Contact angle measurement was performed with a Dataphysics OCA15EC instrument. A water droplet with a volume between 1 and 3 μL was placed on the sample surface, followed by immediate image capturing to measure the static contact angle. Atomic force microscopy (AFM) measurements were carried out on SiO_2 substrates, which were cleaned with acetone.

The electrical conductivity (chemiresistor) properties of nanofibers were characterized under ambient conditions using a Signatone S-1160 Probe Station combined with an Agilent 4156C Precision Semiconductor Parameter Analyzer. The probe station was equipped with a Motic Microscope for positioning and a CCD camera for in situ imaging of the device. The current−time (I−V) curves were measured with a bias voltage of 30 V between the electrodes. The sensor testing experiments were conducted by injecting 5 mL of vapor containing different concentrations of amine over the nanofibers. Diluted aniline vapor was obtained by mixing concentrated vapor with appropriate volume of clean air in a sealed container. The concentration of the diluted vapor was determined by the volume ratio of the concentrated vapor and air. Within the experimental vapor pressure range this dilution method was proven effective for adjusting the aniline concentration.[27]

RESULTS AND DISCUSSION

To achieve uniform coating of FTS molecules onto the nanofibril surface, we used a vapor deposition method (see Figure S1 in the Supporting Information) that was previously developed by others and successfully employed for coating a monolayer of FTS onto molecular crystals and polymer surfaces through cross-linking of the siloxanes.[23,24] This vapor transfer approach is particularly suited for surface coating of nanofibril networks, wherein a large number of nanofibers are intertwined and the interstices formed are hard to reach for solvent (because of surface tension), i.e., difficult to coat through drop casting. Moreover, the solvent-free processing avoids potential damage to the nanofiber (e.g., distortion of the intermolecular arrangement), which often occurs when exposed certain organic solvents.

In this study, we fabricated nanofibers from the DTC molecules (Scheme 1) according to the previously developed method.[17] Because of its strong electron donating property, DTC forms p-type semiconductor as previously evidenced in our lab.[27] Surface doping of DTC nanofibers with electron withdrawing species is expected to enhance the electrical conductivity. Remarkably, the highest occupied molecular orbital (HOMO) of DTC (−4.8 eV) is almost the same as that of rubrene (−4.9 eV) (see Figure S7 in the Supporting Information). This implies that FTS should act as an effective p-type doping for DTC, as it did for rubrene.[23] The doped charge carrier (here the hole) will transport along the long axis of nanofiber through the intermolecular charge delocalization that is enabled by the stacking interaction.[17−22] This combination of effective surface doping and one-dimensional enhanced charge transport would result in significant increase in electrical conductivity. Indeed, as shown in Figure 1, a more than thousand-fold increase in magnitude was obtained for DTC nanofibers upon surface coating with a FTS thin layer.

To confirm the observed conductivity increase is due to the p-type doping of FTS, we performed the same experiment with DTC nanofibers but with coating of a unfluorinated silane, n-octadecyltrichlorosilane (OTS, Scheme 1), which possesses much lower electron affinity than the fluorinated silane. As expected, the electrical conductivity remained almost unchanged upon coating of OTS (Figure 1 and Figure S9 in

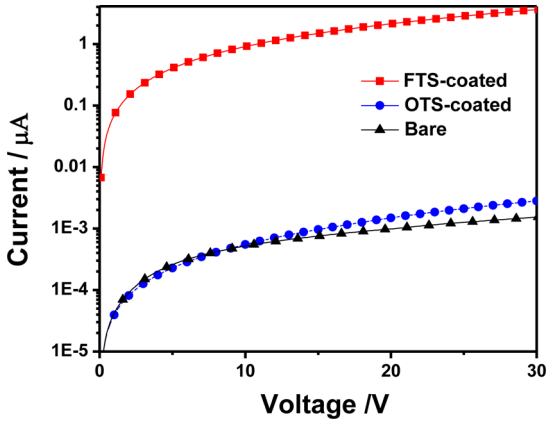

Figure 1. Current–Voltage (I–V) curve for bare, OTS-, and FTS-coated DTC nanofibers. Nanofibers were deposited on a gold electrode pair with a gap of 5 μm and width of 10 μm.

the Supporting Information) due to the lack of charge transfer interaction between DTC and OTS. As discussed above, the effective charge transport pathway along the nanofiber also plays a critical role in the conductivity enhancement. To further prove this role, we fabricated a thin film by drop casting a 15 μM chloroform solution of TDTC (Scheme 1), an analogue of DTC but with longer alkyl side chains. Although the electron donating capability (HOMO level) remains almost the same for the central tetracycle core, the longer side chains of TDTC are not favorable for columnar π–π stacking under conditions of fast evaporation, thus leading to the formation of film structure that lacks extended intermolecular π-stacking, i.e., a nanofibril morphology. Investigation of this thin film under the same FTS coating showed only a few-fold increase in electrical conductivity (see Figure S8 in the Supporting Information). The observed low conductivity is consistent with the poor charge transport within the film material. Similar observation was previously obtained on the photoconductivity of TDTC film upon exposure to oxygen under UV irradiation, for which only slight enhancement of photocurrent was obtained.[27] In contrast, the nanofibers of TDTC (fabricated through solution-based self-assembly) demonstrated 3 orders of magnitude increase in photocurrent under the same measurement conditions.

To further characterize the surface morphology of the DTC nanofibers before and after FTS coating, atomic force microscopy (AFM) was used to image the nanofibril network deposited on the SiO_2 substrate (Figure 2). Both the size and morphology of the nanofibers are consistent with the electronic microscopy imaging performed previously on the same nanofibers.[28] Vapor deposition of the FTS monolayer did not cause any morphology change of the nanofibril structure, indicating that the surface modification is noninvasive to the intermolecular arrangement within the nanofibers. As clearly shown in Figure 2d, the vapor transfer of FTS allowed for interstitial diffusion throughout the nanofibril network and surface deposition onto the bare SiO_2 substrate. Separate investigations proved the effective surface deposition of FTS onto SiO_2 substrate (see the Supporting Information). Such full surface coverage of FTS (on both nanofibers and SiO_2 substrate in between) turned the whole sample surface highly hydrophobic, with a contact angle as large as 136° (see Figure S5 in the Supporting Information). A highly hydrophobic surface prevents the condensation of humidity, thus helping increasing

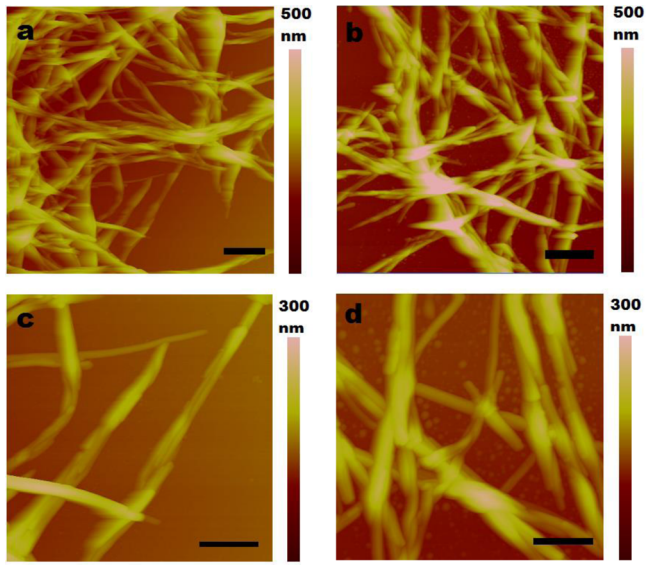

Figure 2. AFM images of DTC fibers (a, c) before and (b, d) after FTS coating. The scale bars are (a, b) 500 nm and (c, d) 200 nm, respectively.

the robustness of the nanofibril materials. Previously, water was found to be detrimental to the electrical conductivity of conducting polymers modified with FTS, causing more than 50% decrease in conductivity when exposed to saturated water vapor.[24] In contrast, the FTS modified DTC nanofibers are sustainable even under saturated water vapor (23 000 ppm) at room temperature (see Figure S11 in the Supporting Information). This water resistance is conducive to development of the nanofibers into ambient sensors.

When deposited on a substrate, the nanofibers form an intertwined network, possessing porosity on a number of length scales depending on the density of nanofibers. The meshlike porosity not only provides increased surface area for enhanced analyte adsorption, but also expedites the diffusion of guest molecules across the film matrix, leading to efficient air sampling of VOCs.[17] Because the surface modification of FTS does not change the global morphology of DTC nanofibers, we expected that the FTS modified DTC nanofibers still possess the large porosity and wide interface as the bare nanofibers, which were previously proven efficient for trace vapor sensing of explosives through fluorescence quenching.[28,29] The high dark conductivity obtained here for the FTS modified DTC nanofibers would ease the use of these nanofibers directly as chemiresistor sensors, for which the high electrical current is conducive to the enhancement of signal-to-noise ratio. Compared to fluorescence sensors, which demand installation and alignment of both excitation light source and photon detector, chemiresistor sensor simply relies on electrical current modulation that can be performed with a micrometer-size electrode pair, thereby facilitating miniaturization of the whole sensor system. Unfortunately, most of the organic nanofiber chemiresistor sensors reported thus far still suffer from the low current, which causes hard to control fluctuation under ambient conditions due to the effect of oxygen.[6,27]

Figure 3 shows the electrical current measured over the FTS modified DTC nanofibers in response to the diluted vapor of aniline. Aniline, with saturated vapor pressure of 880 ppm under ambient conditions, represents one of the common organic amines that have been widely used in various industries.

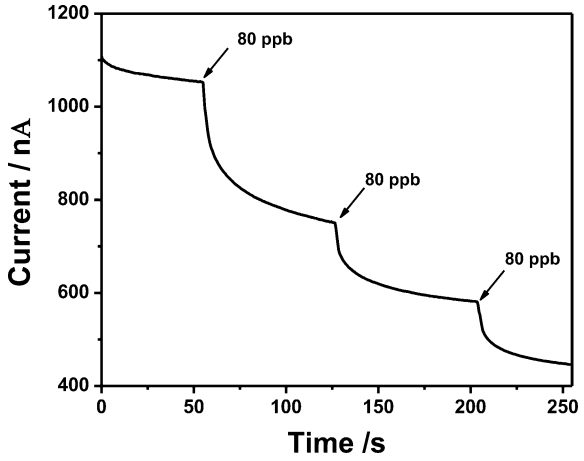

Figure 3. Electrical current measured over the FTS modified DTC nanofibers upon successive exposure to 80 ppb aniline vapor. Nanofibers were deposited on the same electrodes as in Figure 1 and measured under 30 V bias.

Successive exposure to 80 ppb aniline vapor resulted in significant decrease in current. By measuring the current decrease under varying vapor concentrations of aniline and fitting the data with Langmuir adsorption model, we can project the detection limit for aniline vapor down to 0.38 ppb (see the Supporting Information), for which we set the detectable current change as three times the standard deviation of the current measurement (1 nA) under our experimental condition. This detection limit is about 6 orders of magnitude lower than the saturated vapor of aniline. Such high sensitivity of VOC detection is quite rare for chemiresistor based sensors. The high sensing sensitivity obtained for FTS modified DTC nanofibers is largely due to the three-dimensional mesh network of formed by the nanofibers in combination with the strong interfacial interaction between aniline and the nanofiber. While the former enhances the vapor sampling, the latter produces effective charge depletion from the nanofiber. The strong surface adsorption of aniline is also consistent with the fast sensor response as observed, i.e., as shown in Figure 3 and Figures S6 and S10 in the Supporting Information, the current decreases in the time scale of 2.8 s upon exposure to aniline vapor.

Though the detailed chemistry of the surface adsorption of aniline is not completely clear, it is most likely that aniline binds directly with FTS through charge transfer interaction, considering the strong electron donating capability of aniline, with HOMO of −5.6 eV.[30] The binding of aniline thereby decreases the electron affinity of FTS, which in turn weakens the charge separation with DTC. The overall result is that binding of aniline depletes the charge carriers (holes) of DTC nanofiber. The strong binding of aniline within the nanofibril network is also consistent with the fact that no sensor recovery was observed after removal of aniline vapor. Moreover, the nanofibril composite sensor also demonstrates high selectivity for amines, by giving no response to other common organic solvents and reagents as shown in Figure S6 in the Supporting Information. The same FTS modified DTC nanofibers were also tested for vapor sensing against other organic amines (see Table S1 in the Supporting Information) following the same procedure as employed in Figure 3. Similar to the response to aniline, the nanofibers demonstrated significant conductivity modulation upon exposure to the diluted vapor of both aliphatic and aromatic amines (see Table S1 in the Supporting Information), indicating that the reported nanofiber composite functions as a general amine sensor, in the similar manner as the inorganic n-type semiconductor chemiresistors.

CONCLUSION

High dark electrical conductivity was obtained for a p-type organic nanofibril material simply through a one-step surface coating (doping) of electron withdrawing molecules. The nanofibril composite thus fabricated has been proven robust under ambient conditions. The high conductivity, combined with the intrinsic large surface area of nanofibers, enables the development of chemiresistor sensors for trace vapor detection of amines, with detection limits down to sub-parts per billion range. The reported work represents a simple approach to the fabrication of highly conductive nanofibril materials, which may find broad application in sensors and other electronic systems.

ASSOCIATED CONTENT

Supporting Information

Vapor deposition setup, contact angle measurement results, and additional characterization data (PDF). This material is available free of charge via the Internet at http://pubs.acs.org.

AUTHOR INFORMATION

Corresponding Author

*E-mail: jsmoore@illinois.edu (J.S.M.); lzang@eng.utah.edu (L.Z.).

Present Address

[§]D.E.G. is currently at Department of Chemistry, Sam Houston State University, Box 2117, Huntsville, TX 77341, United States

Notes

The authors declare no competing financial interest.

ACKNOWLEDGMENTS

This work was supported by DHS (2009-ST-108-LR0005) and NSF (CHE 0931466). H.H. thanks Dr. Yanke Che for helpful discussion.

REFERENCES

(1) Weiss, D. S.; Abkowitz, M. *Chem. Rev.* **2009**, *110*, 479−526.
(2) Gong, X.; Tong, M.; Xia, Y.; Cai, W.; Moon, J. S.; Cao, Y.; Yu, G.; Shieh, C. L.; Nilsson, B.; Heeger, A. J. *Science* **2009**, *325*, 1665−1667.
(3) Konstantatos, G.; Sargent, E. H. *Nat. Nanotechnol.* **2010**, *5*, 391−400.
(4) Yamamoto, Y.; Fukushima, T.; Suna, Y.; Ishii, N.; Saeki, A.; Seki, S.; Tagawa, S.; Taniguchi, M.; Kawai, T.; Aida, T. *Science* **2006**, *314*, 1761−1764.
(5) Zhu, H.; Li, T.; Zhang, Y.; Dong, H.; Song, J.; Zhao, H.; Wei, Z.; Xu, W.; Hu, W.; Bo, Z. *Adv. Mater.* **2010**, *22*, 1645−1648.
(6) Che, Y.; Yang, X.; Liu, G.; Yu, C.; Ji, H.; Zuo, J.; Zhao, J.; Zang, L. *J. Am. Chem. Soc.* **2010**, *132*, 5743−5750.
(7) de la Escosura, A.; Janssen, P. G. A.; Schenning, A. P. H. J.; Nolte, R. J. M.; Cornelissen, J. J. L. M. *Angew. Chem., Int. Ed.* **2010**, *49*, 5335−5338.
(8) Zhang, X.; Jie, J.; Zhang, W.; Zhang, C.; Luo, L.; He, Z.; Zhang, X.; Zhang, W.; Lee, C.; Lee, S. *Adv. Mater.* **2008**, *20*, 2427−2432.
(9) Yamamoto, Y.; Zhang, G.; Jin, W.; Fukushima, T.; Ishii, N.; Saeki, A.; Seki, S.; Tagawa, S.; Minari, T.; Tsukagoshi, K.; Aida, T. *Proc. Natl. Acad. Sci., U.S.A.* **2009**, *106*, 21051−21056.
(10) Charvet, R.; Acharya, S.; Hill, J. P.; Akada, M.; Liao, M.; Seki, S.; Honsho, Y.; Saeki, A.; Ariga, K. *J. Am. Chem. Soc.* **2009**, *131*, 18030−18031.
(11) Clarke, T. M.; Durrant, J. R. *Chem. Rev.* **2010**, *110*, 6736−6767.

(12) Günes, S.; Neugebauer, H.; Sariciftci, N. S. *Chem. Rev.* **2007**, *107*, 1324−1338.
(13) Placencia, D.; Wang, W.; Shallcross, R. C.; Nebesny, K. W.; Brumbach, M.; Armstrong, N. R. *Adv. Funct. Mater.* **2009**, *19*, 1913−1921.
(14) Yang, F.; Shtein, M.; Forrest, S. R. *Nat. Mater.* **2005**, *4*, 37−41.
(15) Neuteboom, E. E.; Meskers, S. C. J.; van Hal, P. A.; van Duren, J. K. J.; Meijer, E. W.; Janssen, R. A. J.; Dupin, H.; Pourtois, G.; Cornil, J.; Lazzaroni, R.; Brédas, J.-L.; Beljonne, D. *J. Am. Chem. Soc.* **2003**, *125*, 8625−8638.
(16) Che, Y.; Huang, H.; Xu, M.; Zhang, C.; Bunes, B. R.; Yang, X.; Zang, L. *J. Am. Chem. Soc.* **2011**, *133*, 1087−1091.
(17) Zang, L.; Che, Y.; Moore, J. S. *Acc. Chem. Res.* **2008**, *41*, 1596−1608.
(18) Coropceanu, V.; Cornil, J.; da Silva Filho, D. A.; Olivier, Y.; Silbey, R.; Brédas, J.-L. *Chem. Rev.* **2007**, *107*, 926−952.
(19) Che, Y.; Datar, A.; Yang, X.; Naddo, T.; Zhao, J.; Zang, L. *J. Am. Chem. Soc.* **2007**, *129*, 6354−6355.
(20) Sofos, M.; Goldberger, J.; Stone, D. A.; Allen, J. E.; Ma, Q.; Herman, D. J.; Tsai, W.-W.; Lauhon, L. J.; Stupp, S. I. *Nat. Mater.* **2009**, *8*, 68−75.
(21) Delgado, M. C. R.; Kim, E.-G.; Filho, D. t. A. d. S.; Bredas, J.-L. *J. Am. Chem. Soc.* **2010**, *132*, 3375−3387.
(22) Messmore, B. W.; Hulvat, J. F.; Sone, E. D.; Stupp, S. I. *J. Am. Chem. Soc.* **2004**, *126*, 14452−14458.
(23) Calhoun, M. F.; Sanchez, J.; Olaya, D.; Gershenson, M. E.; Podzorov, V. *Nat. Mater.* **2008**, *7*, 84−89.
(24) Kao, C. Y.; Lee, B.; Wielunski, L. S.; Heeney, M.; McCulloch, I.; Garfunkel, E.; Feldman, L. C.; Podzorov, V. *Adv. Funct. Mater.* **2009**, *19*, 1906−1911.
(25) Zhang, W.; Moore, J. S. *J. Am. Chem. Soc.* **2004**, *126*, 12796−12796.
(26) Gross, D. E.; Moore, J. S. *Macromolecules* **2011**, *44*, 3685−3687.
(27) Che, Y.; Yang, X.; Zhang, Z.; Zuo, J.; Moore, J. S.; Zang, L. *Chem. Commun.* **2010**, *46*, 4127−4129.
(28) Che, Y.; Gross, D. E.; Huang, H.; Yang, D.; Yang, X.; Discekici, E.; Xue, Z.; Zhao, H.; Moore, J. S.; Zang, L. *J. Am. Chem. Soc.* **2012**, *134*, 4978−4982.
(29) Naddo, T.; Che, Y.; Zhang, W.; Balakrishnan, K.; Yang, X.; Yen, M.; Zhao, J.; Moore, J. S.; Zang, L. *J. Am. Chem. Soc.* **2007**, *129*, 6978−6979.
(30) Che, Y.; Yang, X.; Loser, S.; Zang, L. *Nano Lett.* **2008**, *8*, 2219−2223.